LETTERS
https://doi.org/10.1038/s41567-019-0584-7

nature physics

High-harmonic generation from an epsilon-near-zero material

Yuanmu Yang[1*], Jian Lu[2], Alejandro Manjavacas[3], Ting S. Luk[4,5], Hanzhe Liu[2], Kyle Kelley[6], Jon-Paul Maria[6], Evan L. Runnerstrom[6], Michael B. Sinclair[4], Shambhu Ghimire[2] and Igal Brener[4,5*]

High-harmonic generation (HHG) is a signature optical phenomenon of strongly driven, nonlinear optical systems. Specifically, the understanding of the HHG process in rare gases has played a key role in the development of attosecond science[1]. Recently, HHG has also been reported in solids, providing novel opportunities such as controlling strong-field and attosecond processes in dense optical media down to the nanoscale[2]. Here, we report HHG from a low-loss, indium-doped cadmium oxide thin film by leveraging the epsilon-near-zero (ENZ) effect[3–8], whereby the real part of the material's permittivity in certain spectral ranges vanishes, as well as the associated large resonant enhancement of the driving laser field. We find that ENZ-assisted harmonics exhibit a pronounced spectral redshift as well as linewidth broadening, resulting from the photo induced electron heating and the consequent time-dependent ENZ wavelength of the material. Our results provide a new platform to study strong-field and ultrafast electron dynamics in ENZ materials, reveal new degrees of freedom for spectral and temporal control of HHG, and open up the possibilities of compact solid-state attosecond light sources.

Although traditionally observed in rare-gas atoms[9], HHG has also recently been reported in a range of solid-state systems[2] including dielectrics[10,11], semiconductors[12,13] and emerging two-dimensional materials[14,15], thus opening up new avenues for solid-state attosecond spectroscopy[10], with the additional advantage of producing stable light waveforms[10,16] in the EUV regime with a compact set-up. Unfortunately, strong above-bandgap absorption restricts the observed solid-state HHG process to a very thin layer of the material (typically tens of nanometres in thickness), significantly limiting the generation efficiency[17].

Nanostructures with plasmonic resonances are widely known to provide enhancements of the optical near field, and therefore have been investigated for boosting the HHG efficiency in the surrounding media[18,19]. However, plasmonic nanostructures typically exhibit a relatively low damage threshold under intense laser fields and the electric field enhancement is restricted to small regions, for example near the apex of conical structures[18]. Furthermore, the periodic arrangement of plasmonic antennas may lead to multiple diffraction of the generated high-harmonic signal over a wide range of angles[12,19], making the collection of high harmonics unwieldy. More recently, materials that exhibit a vanishing real part of their permittivity in certain spectral ranges, commonly known as epsilon-near-zero (ENZ) materials, have been found to exhibit unique nonlinear optical properties[3–8]. Although not yet explored, ENZ materials are appealing for HHG as the ENZ effect can greatly boost the pump laser field over the entire volume of a planar thin film made of the ENZ material. In addition, the deep sub-wavelength thickness of the film may allow efficient extraction of the harmonic signal, thus enhancing the HHG efficiency. Moreover, upon ultrafast high field excitation, the unique hot-electron dynamics of the ENZ material may lead to intriguing spectral and temporal control of the high harmonics.

In this Letter, we report harmonic generation up to the ninth order directly from an ENZ material: In-doped CdO. The sample, as illustrated in Fig. 1a, is formed from a 75-nm-thick In-doped CdO layer epitaxially grown on a (100)-oriented MgO substrate by high power impulse magnetron sputtering[20,21]. The thickness of the CdO film is comparable to its skin depth at the ultraviolet wavelengths of the high-harmonic radiation (see Supplementary Information). An additional 200-nm-thick gold film is then coated on top of the CdO film to increase the confinement of the excitation optical field in the CdO device layer. The In-doped CdO film has a measured carrier density of $2.8\times10^{20}\,\mathrm{cm}^{-3}$ and an electron mobility of $300\,\mathrm{cm}^2\,\mathrm{V}^{-1}\,\mathrm{s}^{-1}$. According to the Drude dispersion formula for this material, the real part of its permittivity crosses zero at a wavelength of 2.1 μm.

The origin of the field enhancement near the material's ENZ wavelength can be intuitively understood by the boundary condition of electromagnetic fields. Specifically, it requires continuity of the normal displacement field $\varepsilon_{\mathrm{MgO}}E_{\mathrm{MgO}}=\varepsilon_{\mathrm{CdO}}E_{\mathrm{CdO}}$ ($\varepsilon_{\mathrm{MgO}}$ and $\varepsilon_{\mathrm{CdO}}$ are the permittivities of MgO and CdO, respectively, and E_{MgO} and E_{CdO} are the normal electric fields at the material boundary). When the real part of $\varepsilon_{\mathrm{CdO}}$ vanishes, E_{CdO} diverges in the limit that the imaginary part of $\varepsilon_{\mathrm{CdO}}$ approaches zero. In-doped CdO has an imaginary permittivity of 0.18 at its ENZ wavelength (Fig. 1b), which is about three times lower than the imaginary permittivity of conventional conductive metal oxides such as ITO at their corresponding ENZ wavelength[21,22]. The lower imaginary permittivity of CdO is enabled by its high crystal quality and higher electron mobility, which is critical for the large field enhancement. Furthermore, the ENZ wavelength can be varied by adjusting the doping level of the CdO film[20]. Figure 1c presents the measured absolute absorption spectra of the sample under *p*- and *s*-polarized incidence, respectively.

[1]State Key Laboratory of Precision Measurement Technology and Instruments, Department of Precision Instrument, Tsinghua University, Beijing, China. [2]Stanford PULSE Institute, SLAC National Accelerator Laboratory, Menlo Park, CA, USA. [3]Department of Physics and Astronomy, University of New Mexico, Albuquerque, NM, USA. [4]Sandia National Laboratories, Albuquerque, NM, USA. [5]Center for Integrated Nanotechnologies, Sandia National Laboratories, Albuquerque, NM, USA. [6]Department of Materials Science and Engineering, North Carolina State University, Raleigh, NC, USA.
*e-mail: ymyang@tsinghua.edu.cn; ibrener@sandia.gov

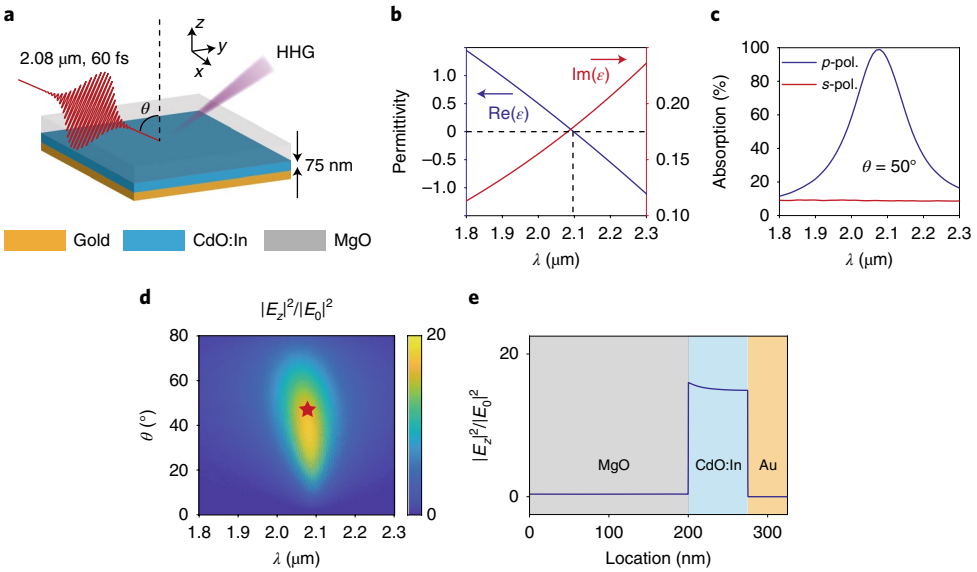

Fig. 1 | Sample schematic and linear optical responses. a, Schematic of the ENZ sample composed of a MgO substrate, CdO thin film and gold capping layer. The pump laser is incident from the substrate side with an incident angle of θ in free space. **b**, Measured real and imaginary parts of the permittivity of CdO as a function of wavelength. **c**, Measured polarization-dependent linear absorption spectra of the sample. **d**, Field enhancements in CdO for *p*-polarized light as a function of wavelength and incident angle calculated from the transfer matrix method. E_0 is the incident electric field in free space. **e**, Calculated field enhancements of the three-layer structure as a function of location at wavelength $\lambda = 2.08\,\mu m$ and $\theta = 50°$ (marked with a red star in **d**).

The absorption peak under *p*-polarized incidence can be attributed to the Ferrell–Berreman resonance, which was first discovered at the ENZ wavelengths of noble metals[23] and polar crystals[24]. Figure 1d illustrates the field enhancements as a function of the wavelength and incidence angle calculated from the transfer matrix method, showing an intensity enhancement of up to 16-fold when the pump wavelength is tuned to the ENZ wavelength. The enhancement factor is inversely proportional to the film thickness[25]. Moreover, as illustrated in Fig. 1e, the field enhancement drops off sharply in the regions outside the ENZ region, indicating that the nonlinear optical response of the structure is boosted dominantly in the ENZ material itself.

We generate high-harmonic radiation by illuminating the sample at an angle of incidence θ with a linearly polarized, 60 fs laser pulse at a 1 kHz repetition rate. The emitted harmonic radiation propagates along the specular reflection direction, collinear with the pump beam (see Methods). Figure 2a shows the high-harmonic spectra obtained from the layered structure under *p*- and *s*-polarized illumination at $\theta = 50°$, with the excitation wavelength λ_0 centred at 2.08 μm. For *p*-polarized illumination, odd-order harmonics are observed from the third to the ninth order, corresponding to a shortest harmonic wavelength of ~250 nm, for a vacuum peak intensity of 14.1 GW cm^{-2} (corresponding to a vacuum field strength of 0.33 V nm^{-1}). Due to the large resonant field enhancement in the ENZ material, this excitation intensity is much weaker than the typical intensity of ~1 TW cm^{-2} used for HHG from zinc oxide and silicon[11,13]. The greatly reduced pump threshold allows the generation of HHG in the ENZ material at a much higher repetition rate, potentially leading to a high-power HHG-based source in the future. In contrast, for *s*-polarized illumination, a configuration that does not lead to field enhancements, no harmonic signal above the third order is observed. The measured third-harmonic yield for *p*-polarized illumination is 482 times greater than that for *s*-polarized illumination. These results serve as clear evidence that HHG originates in the CdO film and is enhanced by the ENZ effect. We do not observe even-order harmonics in any given sample orientation or pump polarization due to the inversion symmetry of CdO's cubic crystal structure[26]. In Fig. 2b, we show the harmonic yield as a function of the excitation intensity. Although the third harmonic for *s*-polarized illumination scales as I^3, where I is the incident laser intensity (an indication of a perturbative effect), the third to the seventh harmonics for *p*-polarized illumination all significantly deviate from perturbative scaling and exhibit a gradual saturation. The harmonic yield is reversible after repeated measurements with pump intensity beyond 11.3 GW cm^{-2}, indicating no permanent damage (see Supplementary Information).

To confirm the resonant nature of HHG in the ENZ sample, we measure the fifth harmonic yield with the central wavelength of the excitation pulse tuned across the CdO ENZ wavelength of 2.1 μm under an identical vacuum intensity of 5.6 GW cm^{-2} (corresponding to a vacuum field strength of 0.2 V nm^{-1}), as illustrated in Fig. 3. Despite the as-expected resonant enhancement of harmonic yield near the ENZ wavelength, we note that the peak of the harmonic yield redshifts to an incident wavelength of 2.13 μm. The redshift of the harmonic peak can be explained by the unique hot-electron dynamics in CdO, as will be detailed in the following.

On careful examination of the harmonic spectra in Fig. 2a, we find that all the harmonic peaks exhibit substantial, excitation intensity-dependent, red-shifts away from the expected harmonic photon energy $N\hbar\omega_0$, the product of the fundamental photon energy $\hbar\omega_0$ and the harmonic order N, where $\hbar$ is the reduced Planck constant. The measured Nth harmonic peak appears at approximately $N \times 0.93\hbar\omega_0$ for all harmonic orders. In Fig. 4a, we present the measured fifth harmonic spectra from the ENZ sample as a function of the excitation intensity. The resonantly enhanced harmonic peak from the ENZ material exhibits a pronounced redshift as the excitation intensity increases, and the redshift saturates at an excitation intensity of 11.3 GW cm^{-2} (corresponding to a vacuum field strength of 0.29 V nm^{-1}). Moreover, we compare the third-harmonic spectrum of the layered structure under resonant *p*-polarized excitation and non-resonant *s*-polarized excitation, and observe that the resonantly enhanced harmonic peak exhibits a

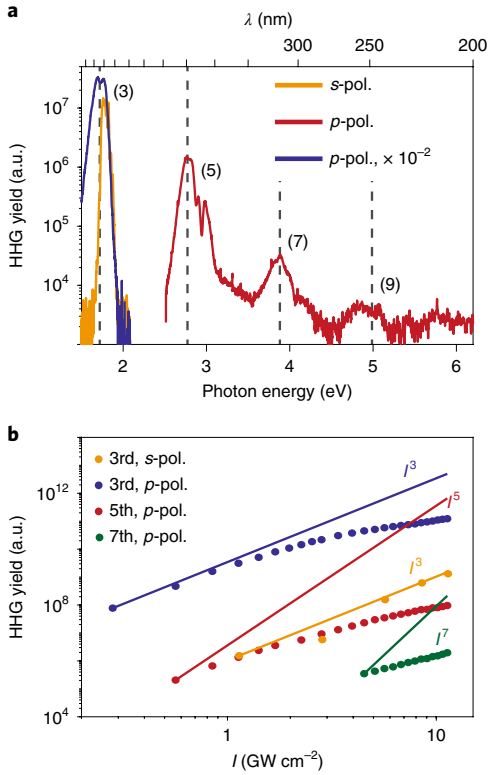

Fig. 2 | HHG from CdO. a, High-harmonic spectrum of the CdO-based structure. For *p*-polarized illumination, the spectrum extends from the third to the ninth order (blue and red line). For *s*-polarized illumination, only third-harmonic generation is observed (orange line). $\hbar\omega_0 = 0.6$ eV is the pump photon energy. Grey dashed lines, photon energy of $N \times 0.93\,\hbar\omega_0$, where N is the harmonic order, specified by the number in parentheses near the harmonic peaks. **b**, Harmonic yield as a function of pump intensity. For *p*-polarized illumination, the third to the seventh harmonics all scale non-perturbatively (blue, red and green dots). For *s*-polarized illumination, the third-harmonic generation scales perturbatively (orange dots). Solid lines show the power scaling law I^N, and are plotted to guide the eye.

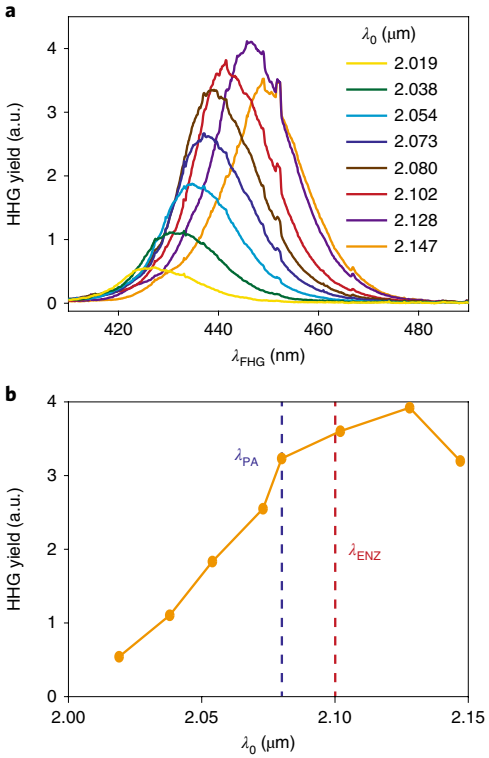

Fig. 3 | Pump wavelength-dependent HHG. a, Fifth-harmonic spectra as a function of excitation wavelength λ_0, with an identical pump intensity of 5.6 GW cm^{-2} (corresponding to a vacuum field strength of 0.2 V nm^{-1}). **b**, Fifth-harmonic yield as a function of λ_0. Harmonic yield is determined by integrating the measured fifth-harmonic spectra. λ_0 is determined by the third-harmonic spectral peak of a bare silicon wafer multiplied by three. The blue dashed line marks the perfect absorption wavelength λ_{PA} of the structure, and the red dashed line marks the ENZ wavelength λ_{ENZ} of CdO.

broadening as large as 1.71 times. This unique feature of linewidth broadening could be used to tailor or reduce the temporal duration of HHG pulses.

We attribute the microscopic origin of the spectral redshift and broadening of the harmonic radiation to the photo induced heating of electrons in the conduction band and the consequent time-dependent ENZ wavelength of the CdO film. As schematically illustrated in Fig. 4b, following sub-bandgap optical excitation, conduction band electrons in CdO are heated to a much higher temperature T_e. The electron heating leads to a modulation of the effective electron mass in CdO and a redshift of CdO's ENZ wavelength, according to the Drude formula[27–29]. The timescale of the modulation is sub-picosecond, and is comparable to the dwell time of the excitation pulse inside the CdO cavity[8], thus leading to a unique feature in our system that the excitation pulse interacts with a time-variant cavity while emitting harmonics. This is manifested in the observed redshift and linewidth broadening of the time-averaged HHG intensity profile. Here, we develop a model to estimate the harmonic spectral peak and bandwidth (see Supplementary Information). We calculate the time-dependent nonlinear current following the pump field being enhanced and modulated by the ENZ cavity at a given excitation intensity and obtain the harmonic spectra from Fourier transformation of the nonlinear current. Figure 4c presents the calculated fifth-harmonic spectra with increasing excitation intensities, which show progressively increasing spectral redshift and broadening, in qualitative agreement with the experimental results. The time-dependent resonant wavelength of the cavity, λ_R, is schematically shown in Fig. 4d, and is determined from a pump–probe measurement[8]. Such a time-averaged model also predicts a non-Lorentzian line-shape of the fifth-harmonic spectra, as is observed in the experiment. We observe a similar spectral redshift and broadening in the third-harmonic spectra with *p*-polarized incidence (see Supplementary Information). At moderately high excitation intensities, a second spectral peak corresponding to non-resonant harmonic generation emerges at a photon energy close to $5\hbar\omega_0$, which is attributed to harmonic emission before the buildup of the resonant cavity.

The temporal and spectral properties of high harmonics can be further manipulated, for example by introducing a frequency chirp to the pump pulse and matching the instantaneous laser frequency to the temporal evolution of the ENZ frequency. HHG can also serve as an ultrafast probe into unique nonlinear processes in various ENZ materials. The ENZ frequency of CdO is tunable from the near- to mid-infrared by adjusting its doping level either chemically or by electrostatic gating, which means that experiments can be performed at other wavelengths. Finally, because conductive metal oxides such as CdO can be integrated within silicon photonics[30], there is a possibility of ultra-compact on-chip EUV and attosecond light sources.

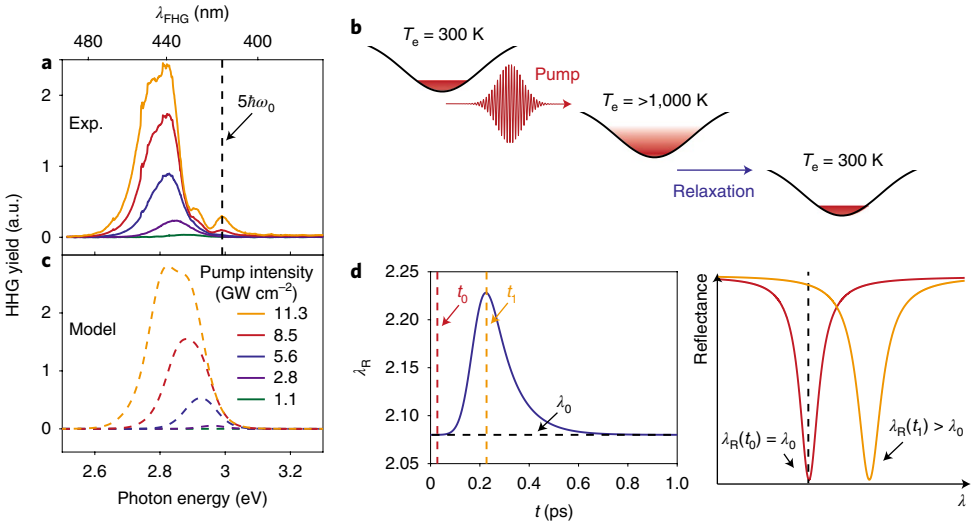

Fig. 4 | HHG spectral shift and broadening. a, Measured spectra of fifth-harmonic generation (FHG) for *p*-polarized illumination as a function of pump intensity. Black dashed line, photon energy of $5\hbar\omega_0$, where $\hbar\omega_0 = 0.6$ eV is the pump photon energy. **b**, Schematics of the hot-electron dynamics of CdO on photo excitation. **c**, Calculated spectra of fifth-harmonic generation for *p*-polarized illumination as a function of pump intensity. **d**, The evolution of the cavity resonance wavelength λ_R as a function of time *t*.

Online content

Any methods, additional references, Nature Research reporting summaries, source data, statements of code and data availability and associated accession codes are available at https://doi.org/10.1038/s41567-019-0584-7.

Received: 8 April 2019; Accepted: 5 June 2019;
Published online: 15 July 2019

References

1. Krausz, F. & Ivanov, M. Attosecond physics. *Rev. Mod. Phys.* **81**, 163–234 (2009).
2. Ghimire, S. & Reis, D. A. High-harmonic generation from solids. *Nat. Phys.* **15**, 10–16 (2019).
3. Alam, M. Z., De Leon, I. & Boyd, R. W. Large optical nonlinearity of indium tin oxide in its epsilon-near-zero region. *Science* **352**, 795–797 (2016).
4. Caspani, L. et al. Enhanced nonlinear refractive index in epsilon-near-zero materials. *Phys. Rev. Lett.* **116**, 233901 (2016).
5. Engheta, N. Pursuing near-zero response. *Science* **340**, 286–287 (2013).
6. Luk, T. S. et al. Enhanced third harmonic generation from the epsilon-near-zero modes of ultrathin films. *Appl. Phys. Lett.* **106**, 151103 (2015).
7. Niu, X., Hu, X., Chu, S. & Gong, Q. Epsilon-near-zero photonics: a new platform for integrated devices. *Adv. Opt. Mater.* **6**, 1701292 (2018).
8. Yang, Y. et al. Femtosecond optical polarization switching using a cadmium oxide-based perfect absorber. *Nat. Photon.* **11**, 390–395 (2017).
9. McPherson, A. et al. Studies of multiphoton production of vacuum-ultraviolet radiation in the rare gases. *J. Opt. Soc. Am. B* **4**, 595–601 (1987).
10. Luu, T. T. et al. Extreme ultraviolet high-harmonic spectroscopy of solids. *Nature* **521**, 498–502 (2015).
11. Ghimire, S. et al. Observation of high-order harmonic generation in a bulk crystal. *Nat. Phys.* **7**, 138–141 (2010).
12. Sivis, M. et al. Tailored semiconductors for high-harmonic optoelectronics. *Science* **357**, 303–306 (2017).
13. Liu, H. et al. Enhanced high-harmonic generation from an all-dielectric metasurface. *Nat. Phys.* **14**, 1006–1010 (2018).
14. Liu, H. et al. High-harmonic generation from an atomically thin semiconductor. *Nat. Phys.* **13**, 262–265 (2017).
15. Hafez, H. A. et al. Extremely efficient terahertz high-harmonic generation in graphene by hot Dirac fermions. *Nature* **561**, 507–511 (2018).
16. Garg, M., Kim, H. Y. & Goulielmakis, E. Ultimate waveform reproducibility of extreme-ultraviolet pulses by high-harmonic generation in quartz. *Nat. Photon.* **12**, 291–296 (2018).
17. Ghimire, S. et al. Generation and propagation of high-order harmonics in crystals. *Phys. Rev. A* **85**, 043836 (2012).
18. Han, S. et al. High-harmonic generation by field enhanced femtosecond pulses in metal–sapphire nanostructure. *Nat. Commun.* **7**, 13105 (2016).
19. Vampa, G. et al. Plasmon-enhanced high-harmonic generation from silicon. *Nat. Phys.* **13**, 659–662 (2017).
20. Sachet, E. et al. Dysprosium-doped cadmium oxide as a gateway material for mid-infrared plasmonics. *Nat. Mater.* **14**, 414–420 (2015).
21. Kelley, K. P., Sachet, E., Shelton, C. T. & Maria, J. P. High mobility yttrium doped cadmium oxide thin films. *APL Mater.* **5**, 076105 (2017).
22. Naik, G. V., Kim, J. & Boltasseva, A. Oxides and nitrides as alternative plasmonic materials in the optical range. *Opt. Mater. Express* **1**, 1090–1099 (2011).
23. Stern, E. A. & Ferrell, R. A. Surface plasma oscillations of a degenerate electron gas. *Phys. Rev.* **120**, 130–136 (1960).
24. Berreman, D. W. Infrared absorption at longitudinal optic frequency in cubic crystal films. *Phys. Rev.* **130**, 2193–2198 (1963).
25. Campione, S., Brener, I. & Marquier, F. Theory of epsilon-near-zero modes in ultrathin films. *Phys. Rev. B* **91**, 121408 (2015).
26. Cimino, A. & Marezio, M. Lattice parameter and defect structure of cadmium oxide containing foreign atoms. *J. Phys. Chem. Solids* **17**, 57–64 (1960).
27. Guo, P., Schaller, R. D., Ketterson, J. B. & Chang, R. P. H. Ultrafast switching of tunable infrared plasmons in indium tin oxide nanorod arrays with large absolute amplitude. *Nat. Photon.* **10**, 267–273 (2016).
28. Kane, E. O. Band structure of indium antimonide. *J. Phys. Chem. Solids* **1**, 249–261 (1957).
29. Turchinovich, D., Hvam, J. M. & Hoffmann, M. C. Self-phase modulation of a single-cycle terahertz pulse by nonlinear free-carrier response in a semiconductor. *Phys. Rev. B* **85**, 201304 (2012).
30. Wood, M. G. et al. Gigahertz speed operation of epsilon-near-zero silicon photonic modulators. *Optica* **5**, 233–236 (2018).

Acknowledgements

This work started when Y.Y. was a postdoctoral researcher at Sandia National Laboratories. The work performed at Sandia National Laboratories was supported by the US Department of Energy (DOE), Office of Basic Energy Sciences, Division of Materials Sciences and Engineering, and performed, in part, at the Center for Integrated Nanotechnologies, an Office of Science User Facility operated for the US DOE Office of Science. Sandia National Laboratories is a multi-mission laboratory managed and operated by National Technology and Engineering Solutions of Sandia, a wholly owned subsidiary of Honeywell International, for the US DOE's National Nuclear Security Administration under contract DE-NA-0003525. The views expressed in this article do not necessarily represent the views of the US DOE or the United States Government. The work performed at SLAC was primarily supported by the US DOE, Office of Science, Basic Energy Sciences, Chemical Sciences, Geosciences and Biosciences Division through the Early Career Research Program. Y.Y. acknowledges support from the Youth Thousand Talent program of China. A.M. acknowledges the National Science Foundation (grant ECCS-1710697) and the UNM Center for Advanced Research Computing for providing high-performance computing resources. J.-P.M. acknowledges support from the National Science Foundation (grant CHE-1507947) and Army

Research Office (grants W911NF16-1-0406 and W911NF-16-1-0037). S.G. thanks U. Thumm for stimulating discussions.

Author contributions

Y.Y. conceived the idea. J.L., Y.Y., T.S.L. and H.L. carried out optical measurements. A.M. developed the theory. K.K., J.-P.M. and E.L.R. prepared the sample. All authors contributed to analysing the data and writing the manuscript. I.B., S.G., M.B.S. and J.-P.M. supervised the project.

Competing interests

The authors declare no competing interests.

Additional information

Supplementary information is available for this paper at https://doi.org/10.1038/s41567-019-0584-7.

Reprints and permissions information is available at www.nature.com/reprints.

Correspondence and requests for materials should be addressed to Y.Y. or I.B.

Peer review information: *Nature Physics* thanks Dmitry Turchinovich and the other, anonymous, reviewer(s) for their contribution to the peer review of this work.

Publisher's note: Springer Nature remains neutral with regard to jurisdictional claims in published maps and institutional affiliations.

Methods

HHG measurements. The experimental set-up for measuring the HHG from the ENZ material is shown schematically in the Supplementary Information. The light source is an optical parametric amplifier (OPA, HE-TOPAS-Prime, Light Conversion) pumped by a Ti:sapphire amplifier system (Legend Elite Duo, Coherent) operating at a 1 kHz repetition rate. The 60 fs idler pulse from the OPA, which is tunable from 2.0 to 2.2 μm in wavelength, is loosely focused into the sample at a ~50° angle of incidence. The area of the focal spot on the CdO surface was estimated to be ~0.0297 cm^2 from a knife edge measurement. The high-harmonic beam propagating along the specular reflection direction is collected by a lens and focused into the entrance slit of a spectrometer, which consists of a grating-based monochromator (Acton, VM-504, grating: 300 grooves mm^{-1}) and a charge-coupled device (CCD, Andor DO440). Spectrally resolved high-harmonic signals emerging from the ENZ material are recorded by the CCD. The polarization of the idler pulse is tuned by a half-waveplate and the excitation intensity is controlled by a variable neutral density (ND) filter. The reported spectral signals are not corrected for the efficiency of the spectrometer at different wavelengths or for *s*- or *p*-polarized pump pulses. To characterize the pump-to-harmonic energy conversion efficiency, we spatially isolated the third-harmonic beam using a prism and measured the energy by a photodiode power sensor (Thorlabs S120VC) at a range of pump energies at 2.08 μm. Higher-order harmonic energies were estimated from the measured third-harmonic energy by referring to Fig. 2b. The lower bound of the energy conversion efficiency for the third, fifth and seventh harmonics were determined to be on the order of 10^{-5}, 10^{-8} and 10^{-10}, respectively, at a pump intensity of 11.3 GW cm^{-2}. The loss of the generated harmonic signal in the optical path was not taken into account.

Data availability

The data that support the plots within this paper and other findings of this study are available from the corresponding authors on reasonable request.

nature physics

SUPPLEMENTARY INFORMATION

https://doi.org/10.1038/s41567-019-0584-7

In the format provided by the authors and unedited.

High-harmonic generation from an epsilon-near-zero material

Yuanmu Yang[1*], Jian Lu[2], Alejandro Manjavacas[3], Ting S. Luk[4,5], Hanzhe Liu[2], Kyle Kelley[6], Jon-Paul Maria[6], Evan L. Runnerstrom[6], Michael B. Sinclair[4], Shambhu Ghimire[2] and Igal Brener[4,5*]

[1]State Key Laboratory of Precision Measurement Technology and Instruments, Department of Precision Instrument, Tsinghua University, Beijing, China. [2]Stanford PULSE Institute, SLAC National Accelerator Laboratory, Menlo Park, CA, USA. [3]Department of Physics and Astronomy, University of New Mexico, Albuquerque, NM, USA. [4]Sandia National Laboratories, Albuquerque, NM, USA. [5]Center for Integrated Nanotechnologies, Sandia National Laboratories, Albuquerque, NM, USA. [6]Department of Materials Science and Engineering, North Carolina State University, Raleigh, NC, USA.
*e-mail: ymyang@tsinghua.edu.cn; ibrener@sandia.gov

Supplementary Figures

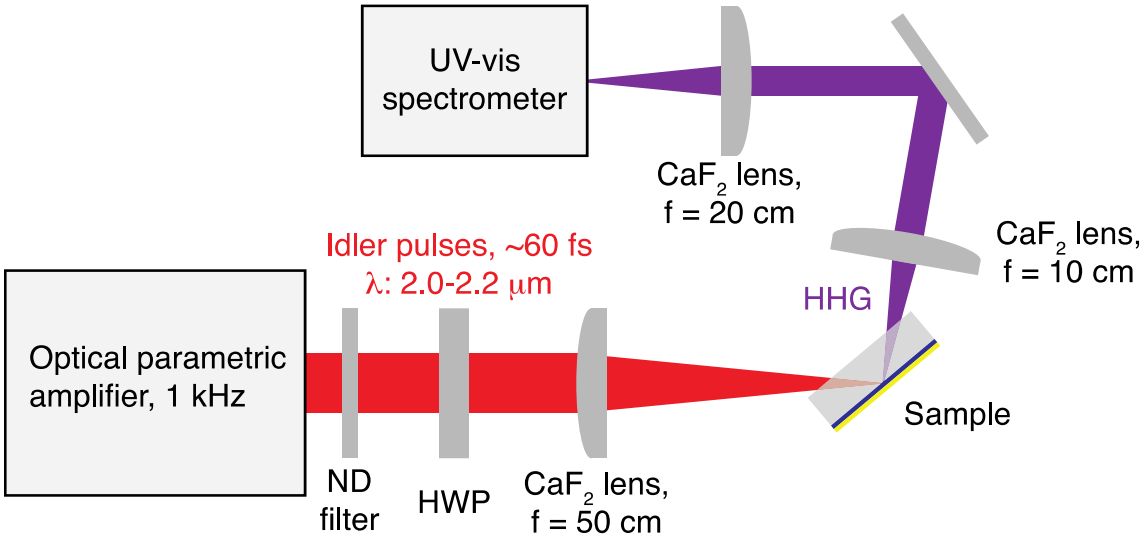

Supplementary Figure 1| Experimental setup for measuring HHG from the ENZ material. ND: neutral density; HWP: half wave-plate.

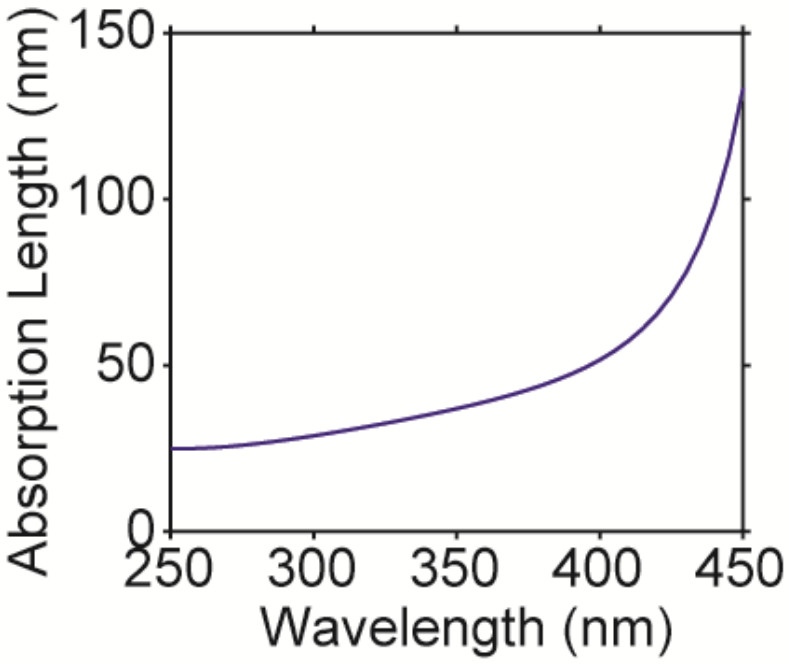

Supplementary Figure 2| UV and visible range absorption length of the CdO thin film measured by spectroscopic ellipsometry.

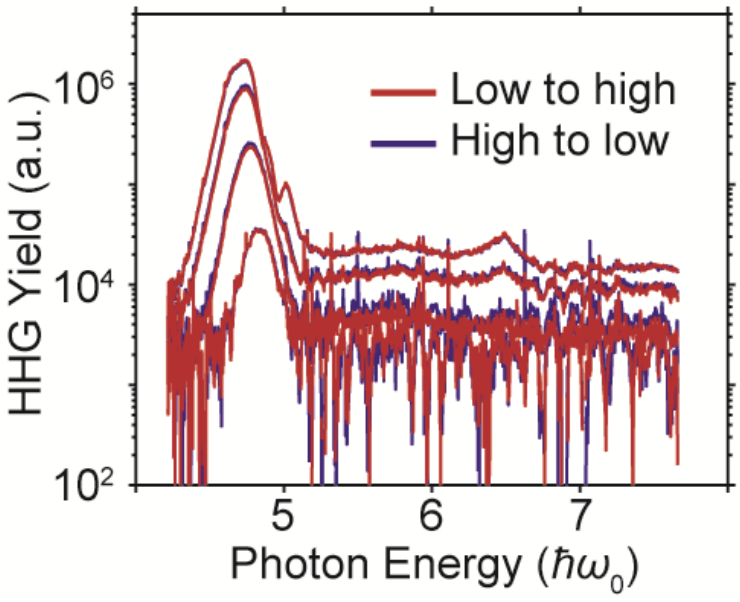

Supplementary Figure 3| The 5th harmonic spectra of the ENZ material with gradually increasing pump intensity (red line) and gradually decreasing pump intensity (blue line), indicating reversible behavior of the sample under intensity laser illumination. The 4 different pump intensities correspond to 1.3 GW cm^{-2}, 2.8 GW cm^{-2}, 5.6 GW cm^{-2}, 8.5 GW cm^{-2}, respectively.

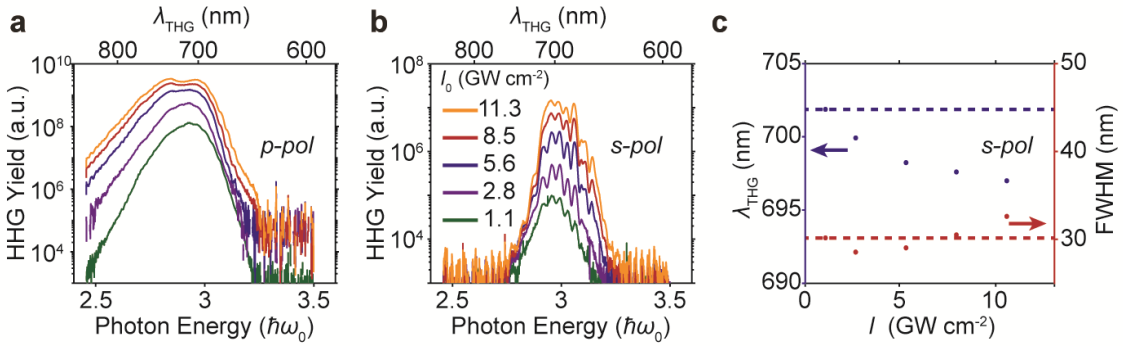

Supplementary Figure 4| a, Spectra of 3rd harmonic generation for *p*-polarized illumination as a function of the pump intensity. **b**, Spectra of 3rd harmonic generation for *s*-polarized illumination as a function of the pump intensity. **c**, Harmonic spectral peak location (blue dot) and spectral FWHM (red dot) as a function of the pump intensity. The Harmonic spectral peak location (blue dashed line) and spectral FWHM (red dashed line) of a bare silicon wafer are also plotted for comparison.

Supplementary Notes

Absorption length of the harmonic radiation

One major drawback of solid-phase UV HHG is the strong absorption of above-gap harmonic emission. Typically, the absorption length is much shorter than the coherent length. The use of an ultra-thin ENZ film as the nonlinear medium can greatly alleviate this issue. From spectroscopic ellipsometry measurements, we determine the absorption length of the CdO thin film as a function of wavelength, as illustrated in Supplementary Fig. 2. The absorption length is comparable with the thickness of the CdO film of 75 nm. We expect that a further reduction of the CdO film thickness may lead to a higher HHG efficiency, due to a stronger field enhancement, as well as a reduced absorption loss.

Reversibility of the HHG measurements

The reversibility of the HHG measurements is shown in Supplementary Fig. 3. We recorded the harmonic spectra at increasing pump intensities and then at identical pump intensities in a decreasing trend. The harmonic spectra at each pump intensity are nearly identical, indicating no damage to the sample throughout these repeated measurements.

Third harmonic spectra of the ENZ sample

In Supplementary Fig. 4a, we show the 3rd harmonic spectra of the ENZ sample under *p*-polarized incidence. Very similar to the 5th harmonic spectra, we observe the spectral red-shift and broadening with increasing pump intensity. However, for *s*-polarized incidence, we instead observe a spectral blue-shift by 0.7%, as shown in Supplementary Figs. 4b and 4c. In addition, we

observe a noticeable spectral interference, which is a result of the multiple reflections of the THG light by the CdO-Au and MgO-CdO interfaces. As the THG light is well below the band gap of CdO, the THG light traverses the CdO film multiple times with negligible loss when it is reflected off of either interfaces. The CdO film with thickness much smaller than the THG wavelength hence acts as a Fabry-Perot interferometer for the THG light. The THG spectrum under *p*-polarized pump pulses also shows spectral modulation, due to the Fabry-Perot interference at relatively low pump intensities. When the pump intensity is sufficiently high, the rapidly evolving instantaneous wavelength of the THG light results in a decrease in the visibility of the interference pattern.

Modeling of the harmonic spectral shift and broadening

Upon illumination by the external laser, the electrons on the CdO film absorb a certain amount of energy per unit of volume and time that can be calculated as

$$P_{\mathrm{abs}} = \frac{\omega}{8\pi}\mathrm{Im}\{\varepsilon_{\mathrm{CdO}}\}|E_{\mathrm{CdO}}|^2 \quad \text{(S1)}$$

where E_{CdO} is the electric field inside of the CdO. By neglecting the component of this field parallel to the film, which is much smaller than the perpendicular one, and assuming that the field is uniform within the CdO layer, we can write

$$|E_{\mathrm{CdO}}|^2 = |f(\omega,\theta)|^2|E_0|^2 \quad \text{(S2)}$$

where $f(\omega,\theta)$ is the field enhancement factor inside the CdO layer, which is calculated using the transfer matrix method, and E_0 is the incident field, which is related to the incident intensity I as

$$|E_0|^2 = \frac{8\pi}{c}\frac{I}{\cos\theta} \text{ (S3)}$$

where θ is the angle of incidence. Then, the total energy absorbed per unit of volume by the CdO electrons can be written as $U_{\text{abs}} = P_{\text{abs}}\Delta t$, where Δt is the pulse duration. This absorbed energy results in an increase of the temperature of the electrons that can be written as

$$\Delta U = U(T_e) - U(T_e = 300\text{K}) = U_{\text{abs}} \ (S4)$$

where $U(T_e)$ is the electron energy density, which can be calculated as[1]

$$U(T_e) = \frac{\sqrt{2}}{\pi^2}\frac{m^{3/2}}{\hbar^3}\int_0^\infty d\mathcal{E}\ \mathcal{E}\left(1+\frac{2\mathcal{E}}{\mathcal{E}_g}\right)\sqrt{\mathcal{E}+\frac{\mathcal{E}^2}{\mathcal{E}_g}}f_0(T_e,\mu) \ (S5)$$

Here, $\mathcal{E}$ is the energy of the electrons, m their effective mass, which we take to be $m = 0.12m_e$, and $f_0(T_e,\mu)$ the Fermi-Dirac distribution for temperature T_e and chemical potential μ. This expression assumes that the non-parabolic band structure of CdO can be described as[2]

$$\frac{p^2}{2m} = \mathcal{E} + \frac{\mathcal{E}^2}{\mathcal{E}_g} \ (S6)$$

with p and $\mathcal{E}_g$ being, respectively, the linear momentum of the electrons and the parameter that characterizes the shape of the electronic band, for which we use a value $\mathcal{E}_g$ = 2.92 eV. The

intraband nature of the pumping process results in the conservation of the electronic density, which in our case is n_e = 2.8×10^{20} cm^{-3}. This allows us to calculate the temperature dependent chemical potential using[1]

$$n_e = \frac{\sqrt{2}}{\pi^2}\frac{m^{3/2}}{\hbar^3}\int_0^\infty d\mathcal{E}\left(1+\frac{2\mathcal{E}}{\mathcal{E}_g}\right)\sqrt{\mathcal{E}+\frac{\mathcal{E}^2}{\mathcal{E}_g}}\,f_0(T_e,\mu) \quad (S7)$$

With these expressions, we can compute the raise of the electron temperature of the electrons produced by the external pump. This increase of temperature produces a change in the plasma frequency of CdO that can be obtained from[1]

$$\omega_p^2(T_e) = \frac{4e^2}{3\pi m}\left(\frac{2m}{\hbar^2}\right)^{3/2}\int_0^\infty d\mathcal{E}\,\frac{\left(\mathcal{E}+\frac{\mathcal{E}^2}{\mathcal{E}_g}\right)^{3/2}}{1+\frac{2\mathcal{E}}{\mathcal{E}_g}}\left(-\frac{\partial f_0(T_e,\mu)}{\partial\mathcal{E}}\right) \quad (S8)$$

where e is the electron charge.

The nonlinear response of the electrons of CdO can be estimated from the time dependent electronic current, which reads

$$j(t) \propto \frac{\partial\mathcal{E}}{\partial p} = \frac{-\frac{e}{\omega m}|f(\omega,\theta)|E_0\sin(\omega t)}{\sqrt{1+\frac{2e^2}{\omega^2 m\mathcal{E}_g}[|f(\omega,\theta)|E_0\sin(\omega t)]^2}} \quad (S9)$$

where ω is the frequency of the pump and we have used the fact that, for a monochromatic electric field oscillating at ω, the linear momentum of the electrons satisfies

$$\frac{\partial p}{\partial t} = -e|f(\omega,\theta)|E_0 \cos(\omega t) \quad (S10)$$

Notice that this current is affected by the change in the plasma frequency of CdO, caused by the increase of T_e, through the field enhancement factor. The intensity of the Nth harmonic can be estimated as

$$I_{N\omega} \propto \left| \omega^2 \int_0^{\frac{\pi}{\omega}} dt\, j(t) \sin(N\omega t) \right|^2 \quad (S11)$$

We use the expressions above to compute the results of Fig. 4c of the main paper. Specifically, we assume the pump is incident at an angle θ = 50º, has a duration of Δt = 60 fs, and has a central frequency of ω_0 = 0.596 eV. Futhermore, the dielectric functions of Au and CdO are described using the Drude model $\varepsilon = \varepsilon_\infty - \omega_p^2/(\omega^2 + i\omega\gamma)$. In the case of Au, we choose $\varepsilon_\infty = 1$, $\hbar\omega_p$= 8.991 eV, and $\hbar\gamma$ = 0.165 eV, while for CdO we take ε_∞= 5.5 and $\hbar\gamma$ = 0.019 eV. Notice that, in this case, the plasma frequency is obtained from the equation discussed above. For T_e= 300 K we obtain $\hbar\omega_p$ = 1.388 eV. With all of these parameters, we can calculate the intensity of the different harmonics emitted by the system. It is important to remark that the electron temperature obtained from Eqs. S1-S7 represents the maximum temperature achievable for the particular pump intensity used in the calculation. However, we know that the high harmonic emission does not happen

exclusively at the maximum electronic temperature. On the contrary, the electrons radiate during the rise and posterior decrease of their temperature. In order to account for this fact and get a better estimate of the high harmonic spectrum, we compute the spectra shown in Fig. 4c of the main paper by averaging the spectra obtained at different temperatures spanning the range between room temperature and the maximum value obtained from Eqs. S1-S7. To perform the average, we assume the electronic temperature follows a temporal evolution identical to the one measured for the change on the resonant wavelength of the system, shown in Fig. 4d of the main paper. Then, we weight the spectra for each of these temperatures using a time-dependent Gaussian profile that accounts for the different intensity of the pump field, and therefore of the electronic excitation, at different times. The results of this average reproduce the measured spectra as can be seen by comparing Figs. 4a and c.

Supplementary References

1 Guo, P., Schaller, R. D., Ketterson, J. B. & Chang, R. P. H. Ultrafast switching of tunable infrared plasmons in indium tin oxide nanorod arrays with large absolute amplitude. *Nature Photonics* **10**, 267 (2016).

2 Kane, E. O. Band structure of indium antimonide. *Journal of Physics and Chemistry of Solids* **1**, 249-261 (1957).